CrystEngComm

ROYAL SOCIETY OF CHEMISTRY

PAPER

View Article Online
View Journal | View Issue

Cite this: *CrystEngComm*, 2022, **24**, 7915

Solubility and permeability enhancement of BCS class IV drug ribociclib through cocrystallization†

M. K. Chaitanya Mannava, [ab] Abhijit Garai, [a] Manish K. Bommaka, [a] K. Anand Solomon *[b] and Ashwini K. Nangia *[a]

Received 17th September 2022,
Accepted 25th October 2022

DOI: 10.1039/d2ce01288j

rsc.li/crystengcomm

Ribociclib (RBC) is an antineoplastic agent and a Biopharmaceutics Classification System (BCS) class IV drug with poor solubility and low permeability. A novel salt form of RBC with vanillic acid (VA) and a cocrystal with resorcinol (RES) were successfully synthesized and, for the first time, the crystal structure of RBC as its hydrate (RBC–HYD) is reported. The synthesized salt hydrate, RBC–VA–HYD, and cocrystal, RBC–RES, were satisfactorily characterized by single crystal X-ray diffraction to show that the two components in 1 : 1 stoichiometry exist in both salt and cocrystal forms, respectively. The dominant hydrogen bonds between RBC and VA are the charge-assisted O–H···O$^-$ and N$^+$–H···O$^-$, whereas in the RBC–RES cocrystal O–H···O and O–H···N hydrogen bonds are present. The solubility, dissolution rate and permeability of the salt and cocrystal were studied under physiological pH environments. RBC in the cocrystal form exhibited 2-fold enhancement in permeability compared to pure RBC. The present investigation not only provides a promising candidate for improved therapeutic activity against cancer, but also provides a direction for selecting between salt or cocrystal forms for a high bioavailability drug formulation.

1. Introduction

Ribociclib (RBC) is an oral dosage antineoplastic agent inhibitor of cyclin dependent kinase specifically for (CDK) 4/6.[1] It is particularly used for the treatment of metastatic breast cancer.[2] Due to its poor aqueous solubility (0.24 mg mL^{-1}) and low permeability (log *P* 2.38), it is classified as a Biopharmaceutical Classification System (BCS) class IV drug.[3] The succinate salt of RBC (RBC–SA) was developed by Novartis (tradename Kisqali®) and it was reported that, despite the drug compound RBC in the succinate salt form increased in solubility, the drug concentration in the gastrointestinal (GI) tract did not improve the absorption rate as the drug molecules have to permeate across the GI tract.[4] Therefore, the 600 mg dosage of the RBC–succinate salt form was formulated which appears to be a high dosage strength for chronic and late-stage cancer patients.[5] If the balance between the solubility and permeability can be optimized to achieve high maximal overall absorption of RBC, then the drug efficacy can be improved at a lower dosage level.[6] A change in crystal lattice energy and solute–solvent interactions could enhance drug solubility and permeability. Cocrystallization is an effective way to influence both the solubility and dissolution profile factors by altering the crystal lattice of the API by introducing a suitable coformer *via* supramolecular synthon formation.[7] Coformers having higher hydrophilicity tend to increase the solvent affinity of the resultant crystalline phase, resulting in better solubility.[8,9] In contrast to numerous reports on the solubility and dissolution profile increase of cocrystals and salts, there are relatively fewer studies on cocrystals which can modulate the flux rate for enhanced permeability of drugs, which affects oral absorption and sustains a high pharmacokinetic profile of the drug substance.[10] Several research groups have demonstrated that cocrystals are able to alter the solubility and the permeability of APIs.[11–13] In a cocrystal drug formulation, the structure and properties of the coformer play a pivotal role and therefore judicious selection of the coformer based on its hydrophilicity and lipophilicity is important to produce a cocrystal with high solubility and high permeability.[14] Also, drug–coformer interactions, crystal packing, and their interplay with the solvent play a decisive role in modulating permeability for an optimal formulation.[15]

A Cambridge Structural Database (CSD)[16,17] search of RBC resulted in only one hit, ribociclib succinate (2 : 1) salt dihydrate DMSO solvate (CCDC No. 2067542).[4] Several crystalline forms of RBC have been reported in patents including polymorphs, succinate salt, and cocrystals. In the

[a] *School of Chemistry, University of Hyderabad, Central University P.O., Prof. C. R. Rao Road, Hyderabad 500046, India. E-mail: ashwini.nangia@gmail.com*
[b] *Department of Chemistry, School of Engineering, Dayananda Sagar University, Kudlu Gate, Bangalore 560 068, India. E-mail: anands-chem@dsu.edu.in*

† Electronic supplementary information (ESI) available: PXRD, IR, crystallographic parameters, hydrogen bond table, tables for solubility, IDR and diffusion. CCDC 2131754–2131756. For ESI and crystallographic data in CIF or other electronic format see DOI: https://doi.org/10.1039/d2ce01288j

scientific articles, cocrystals of RBC were reported with saccharin, cholic acid and orotic acid, whereas, citric acid formed a salt.[8] However, the single crystal X-ray structures of RBC and its cocrystals have not been published. We report herein the RBC hydrate form (RBC–HYD) and two new multicomponent solid forms, a cocrystal with resorcinol (RBC–RES, 1 : 1) and a salt hydrate with vanillic acid (RBC–VA–HYD, 1 : 1 : 1) investigated *via* crystal engineering and solubility and permeability studies of the novel solids. The prepared cocrystal of RBC–RES was found to be stable under stressed conditions and also exhibited enhanced solubility, dissolution, and permeability compared to pure RBC, RBC–HYD and RBC–VA–HYD salt. This improvement in the characteristics is also useful in the processing of the drug formulation with superior bioavailability.

The chemical structure of RBC shows that it contains multiple hydrogen bonding sites such as N-heterocyclic moiety piperazine, amino-pyridine and pyrrole-pyrimidine, and acyclic amine and amide functionalities (Scheme 1). Therefore, from the chemical nature of different moieties present in RBC, it is realized that RBC is a basic drug molecule with pK_a values of 8.87 (strongest base, piperazine moiety), 5.98 (pyrimidine moiety), and 4.44 (pyridine moiety).[18] The physicochemical properties of a drug can be altered through the formation of a cocrystal or salt, and thus judicious selection of a coformer based on acidity/basicity, hydrogen bond donor/acceptor sites, and hydrophilicity/hydrophobicity is important to produce a cocrystal/salt with the desired physicochemical properties. Two generally recognized as safe[19] (GRAS) coformers, *i.e.*, vanillic acid (VA, pK_a 4.16)[18] and resorcinol (RES; pK_a 9.26),[18] were screened to obtain multicomponent solids (Scheme 1). An estimate of ΔpK_a difference is listed in Table 1. The ΔpK_a[19] of vanillic acid and RBC is >3 whereas for resorcinol and RBC, it is <0, indicating the formation of a salt and cocrystal, respectively.[20–23] Our objective was to compare the solubility, dissolution and membrane permeability of the multi-component adducts with the reference drug.

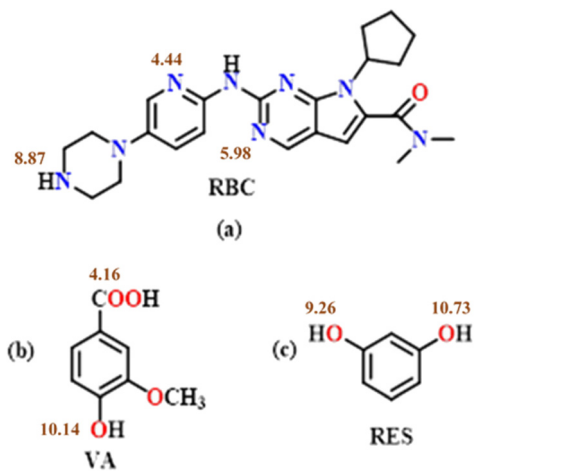

Scheme 1 (a) Chemical structure of ribociclib (RBC) and coformers (b) vanillic acid (VA) and (c) resorcinol (RES). Approximate pK_a values of the functional groups are quoted.

2. Experimental

2.1. Materials

Ribociclib was purchased from Dhiyo Pharma (India), and the purity of the compound was confirmed by PXRD and DSC. The coformers vanillic acid (VA) and resorcinol (RES) were purchased from Sigma-Aldrich, Hyderabad, India, and used as such without further purification. All chemical reagents used were of analytical grade.

2.2. Synthesis and crystallization

2.2.1. Ribociclib hydrate (RBC–HYD, 1 : 1). RBC–HYD was prepared using the slurry method. 100 mg RBC was taken in a round bottom flask and 5 mL of MeOH–H_2O solvent mixture (60 : 40 ratio) was added to it. The slurry was stirred for 24 h, filtered and dried. Single crystals of RBC monohydrate were obtained by slow solvent evaporation using the MeOH–H_2O solvent mixture.

2.2.2. Ribociclib–vanillic acid salt hydrate (RBC–VA–HYD, 1 : 1 : 1). RBC–VA–HYD was prepared using the slurry method. Ribociclib (434 mg, 0.1 mmol) and vanillic acid (168 mg, 0.1 mmol) were taken in a 25 mL round bottom flask and 15 mL of MeOH–H_2O (60 : 40 ratio) solvent mixture was added. The slurry was stirred for 24 h to generate RBC–VA–HYD. The resulting solid powder was used for solution crystallization. RBC–VA–HYD (about 40 mg) was dissolved completely in 15 mL of MeOH–H_2O (60 : 40 ratio) mixture and kept at 60 °C (in a controlled temperature bath) to evaporate the solvent which resulted in the formation of single crystals of RBC–VA–HYD (1 : 1 : 1) within 48 h.

2.2.3. Ribociclib–resorcinol cocrystal (RBC–RES, 1 : 1). Solvent-assisted grinding (for 30 min, using 1 mL MeOH) of RBC (434 mg, 0.1 mmol) and RES (110 mg, 0.1 mmol) with a mortar–pestle produced the RBC–RES cocrystal. The resulting solid powder was used for solution crystallization. About 20 mg of the powder material was dissolved in MeOH (5–6 mL) and kept for slow evaporation (at room temperature) in a glass vial. After 3–4 days, light yellow-colored crystals of RBC–RES were obtained. Resorcinol has been used as a coformer to improve the dissolution, solubility and stability of drug cocrystals.[24–26]

2.3. Single crystal X-ray diffraction

X-ray reflections on the multi-component solid forms were collected on a Bruker SMART APEX CCD diffractometer equipped with a graphite monochromator and a Mo-Kα fine-focus sealed tube (λ = 0.71073 Å) operated at 1500 W power (40 kV, 30 mA). The frames were integrated with Bruker SAINT software using a narrow-frame integration algorithm. Intensities were corrected for absorption effects using the multi-scan method (SADABS), and the structure was solved and refined using SHELX-2014. All non-hydrogen atoms were

Table 1 ΔpK_a values of RBC and coformers

API/coformer	pK_a (strongest base of API and strongest acid of coformer)	ΔpK_a	Molecular complex
RBC	8.87	—	—
RBC–VA	4.16	4.71	1 : 1 salt
RBC–RES	9.26	−0.39	1 : 1 cocrystal

refined anisotropically. Hydrogen atoms on heteroatoms were located from difference electron density maps, and all C–H hydrogens were fixed geometrically.[27,28] Hydrogen-bond geometries were determined in PLATON. A check of the final crystallographic information file (CIF) with PLATON did not show any missed symmetry.[29] (CCDC No. 2131754–2131756).

2.4. Powder X-ray diffraction

Powder X-ray diffraction was recorded on a Bruker D8 Advance diffractometer (Bruker-AXS, Karlsruhe, Germany) using Cu-Kα X-ray radiation (λ = 1.5406 Å) at 40 kV and 30 mA power. X-ray diffraction patterns were collected over the 2θ range of 3–50° at a scan rate of 5° min^{-1}. Powder Cell 2.455 (Federal Institute of Materials Research and Testing, Berlin, Germany) was used for Rietveld refinement of the experimental PXRD and calculated lines from the X-ray crystal structure.

2.5. Vibrational spectroscopy

Infrared spectra of RBC and the complexes were recorded on a Thermo-Nicolet 6700 FT-IR-NIR spectrometer with the KBr pellets of the sample (the sample and KBr were mixed well and compressed using 2.5 ton pressure in a KBr press machine for 3 min to make the pellet). Omnic software (Thermo Scientific, Waltham, MA) was utilized to analyze the data. Each sample was scanned 120 times in the range of 400–4000 cm^{-1}, and the spectra were normalized with background correction. Spectral details are provided in the ESI† (Fig. S1–S3, Table S1).

2.6. Thermal analysis

Differential scanning calorimetry (DSC) was performed on a Mettler-Toledo DSC 822e module (Mettler-Toledo, Columbus, OH) to determine the melting point and thermal events. Thermogravimetry analysis (TGA) was carried out on a Mettler Toledo TGA/SDTA 851e module (Mettler-Toledo, Columbus, OH) to measure any solvent/water release from the crystal lattice. The samples were placed in a sealed pin-pricked aluminum pan for DSC and in an alumina pan for TGA measurement. The characteristic sample size was 3–5 mg for DSC and 4–6 mg for TGA. The temperature range for the heating cycle was 30–300 °C and 30–400 °C for DSC and TGA, respectively. The samples were heated at a rate of 10 °C min^{-1}. All the samples were purged in a stream of dry nitrogen flowing at 50 mL min^{-1} and 80 mL min^{-1} for DSC and TGA, respectively.

2.7. Solubility and dissolution measurements

Solubility measurements[30] of RBC and its adducts were conducted in pH 7 phosphate-buffered saline (PBS) medium. From UV-vis spectroscopy, the λ_{max} of RBC was observed at 260 nm and so, for high-performance liquid chromatography (HPLC) analysis, the wavelength was set at 260 nm. The area under the curve (AUC) values obtained from HPLC analysis for known concentration of RBC were used to plot the calibration curve. The slope and intercept of the calibration curve were used to determine the unknown concentration of RBC. To measure the equilibrium solubility, an excess amount of each sample (*i.e.*, RBC and its hydrate, salt hydrate and cocrystal) was added to 5 mL of PBS medium (pH 7) and stirred at 800 rpm using a magnetic stirrer at 37 °C ± 1 to make the solution saturated. After 24 h, the suspension was filtered through a Whatman 0.45 μm syringe filter. The filtrate was used to calculate the equilibrium solubility from the area under the curve (AUC) plotted against the standard curve of HPLC analysis. The undissolved residues were dried and further characterized by PXRD.

An Electrolab TDT-08L dissolution tester was used to perform pellet dissolution. Dissolution measurements were performed using 200 mg RBC and the same mass of active drug was consistently used for its hydrate (218 mg), salt hydrate RBC–VA–HYD (285 mg) and cocrystal RBC–RES (250 mg). Each compound was taken in 500 mL of pH 7 phosphate buffer saline (PBS) dissolution medium. The pellet rotation was fixed at 100 rpm and dissolution experiments were continued for up to 8 h at 37 °C. At regular intervals, 5 mL of the dissolution medium was withdrawn and replaced by an equal volume of fresh medium to maintain a constant volume and the concentration of the aliquots was quantified by HPLC at 260 nm λ_{max}, and the AUC was calculated by the linear trapezoidal method from 0 to 8 h.

2.8. Diffusion measurements

Diffusion studies were carried out with a glass Franz diffusion cell (Model JFDC-07, Orchid Scientific, Maharashtra, India) with 20 mL volume. A dialysis membrane-135 (width 33.12 mm, diameter 23.8 mm, and capacity 4.45 mL cm^{-1}) purchased from HiMedia, India was used. The dialysis membrane was pre-treated with 2% $NaHCO_3$ at 80 °C for 30 min to remove traces of sulfides, followed by 10 mM of EDTA at 80 °C for 30 min to remove traces of heavy metals and another 30 min of treatment with deionized water at 80 °C to remove glycerin. The treated dialysis membrane was placed between the two compartments fixed by a stainless-steel clamp with an

effective mass transfer area of 3.14 cm^2. The receptor compartment was filled with PBS solution, and air bubbles were removed. The donor compartment was loaded with 20 mg active RBC and its hydrate, salt and cocrystal in equimolar ratio powders (20 mg active RBC drug was maintained in all experiments) and 2 mL of PBS was added. The temperature of the diffusion medium was thermostatically maintained at 37 ± 1 °C throughout the experiment at 600 rpm and it was allowed to diffuse through the membrane towards the receptor compartment. Aliquots of 0.5 mL were withdrawn from the receptor compartment at set time periods (30, 60, 90, 120, 150, 180, 240, 300, 360, 420 min) and fresh PBS was added to replenish the volume. The concentration of the diffused material was determined by HPLC.

2.9. HPLC assay

HPLC analysis was performed on a Shimadzu LC-20AD liquid chromatograph with a photodiode array SPD-M20A detector and a degasser DGU-20A3 using a reverse-phase (RP) HPLC column C18G (250 × 4.6 mm, 5 μm particle size). λ_{max} at 260 nm was used to quantify the RBC drug. The calibration curves were obtained by spiking RBC (linearity $R^2 > 0.999$). MeOH–CH_3CN (50 : 50) was used as mobile phase A and water–acetic acid solution (adjusted to pH 4) was used as mobile phase B with a ratio of 40 : 60, respectively. The solvent was filtered through a 0.45 μm membrane filter, degassed in a sonicator, and delivered at a rate of 1 mL min^{-1}. Solubility, dissolution, and diffusion samples were injected into HPLC with a run time of 10 min.

3. Results and discussion

In the search for a better oral formulation of RBC, a cocrystal with resorcinol and a salt-hydrate with vanillic acid were studied. The presence of COOH and OH hydrogen bond donor groups on the coformers was expected to form strong heterosynthons with the piperazine and aminopyridine groups on the drug, with the ΔpK_a rule guiding the proton state in the acid–base adduct. The cocrystallization of these crystalline materials was carried out using liquid-assisted grinding and slurry methods. Single crystals of the multicomponent solids were obtained by slow solvent evaporation. In our attempt to produce single crystals of pure RBC, we found that the drug crystallized as a monohydrate from the methanol–water solvent. The products were characterized by IR, DSC, TGA, PXRD and SC-XRD techniques, and bulk phase purity was established by PXRD (Fig. S4, ESI†). The equilibrium solubility, intrinsic dissolution rate and permeability profiles of these materials are discussed. Crystallographic and hydrogen bond parameters are summarized in Tables S2 and S3 (ESI†).

3.1. Crystal structure analyses

3.1.1. Ribociclib hydrate (RBC–HYD, 1 : 1). The RBC-hydrate crystallized in the space group $P2_1/n$ with one molecule each of RBC and H_2O in its asymmetric unit. In the crystal structure, the RBC molecule is strongly hydrogen bonded with two water molecules and one RBC molecule, whereas each H_2O is found to participate in strong hydrogen bonding with two RBC molecules. RBC molecules are bonded as dimers through homosynthons of N–H···N hydrogen bonds (2.23 Å, 165°) between the amino-pyridine groups with an $R_2^2(8)$ ring motif[31] (Fig. 1a). A H_2O molecule is connected to two RBC molecules *via* O–H···N (2.03 Å, 160°) and O–H···O (1.87 Å, 164°) hydrogen bonds. In order to analyze a simplified hydrogen-bond network, the centroids of the $R_2^2(8)$

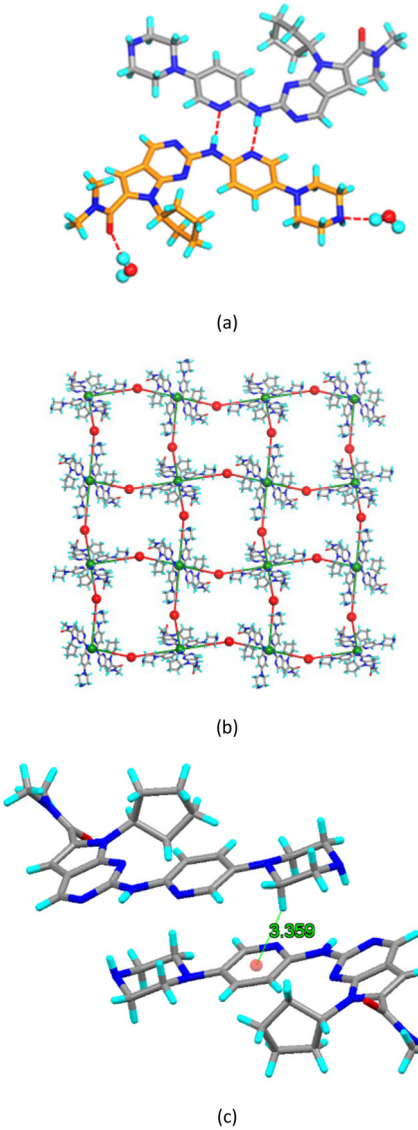

Fig. 1 Crystal structure of RBC–HYD. (a) Hydrogen bonding of the RBC dimer with water molecules; (b) 2D layered network formed *via* hydrogen bonding between RBC and water molecules shown as a square node network; (c) C–H···π interaction between RBC molecules.

ring and the oxygen atom of water molecules were treated as nodes and connected according to the hydrogen bonding interactions to give a square network structure. Each RBC ring node is a four-connected node, as it is connected to four H_2O nodes, and similarly each H_2O node is found to be a two-connected node. Node connections following the hydrogen bonding of RBC and water molecules exhibit the formation of a 2D corrugated layered type network with the smallest unit of an eight membered ring (Fig. 1b). Corrugated layers are found to be slipped stacked where C–H···π (centroid) interactions (3.36 Å) are observed between RBC molecules (Fig. 1c).

3.1.2. Ribociclib–vanillic acid salt hydrate (RBC–VA–HYD, 1 : 1 : 1). The RBC–VA salt hydrate crystallized in the $P2_1/n$ space group and its asymmetric unit contains one molecular ion each of singly protonated RBC and singly deprotonated VA and a water molecule. The presence of a carboxylate group in the coformer is confirmed by C–O bond distances in the COO^- group which are 1.256 Å and 1.264 Å (Δ bond distance $<$0.01 Å, e.s.u. 0.003 Å). The acid proton of VA is transferred to the piperazine N of RBC. The protonated RBC is hydrogen bonded to two deprotonated VA ions and one H_2O (Fig. 2a). Vanillic acid anions are bonded as 1D chains through charge-assisted O–H···O^- hydrogen bonds (1.86 Å, 167°) between the hydroxyl group donor and carboxylate acceptor. These 1D chains are further connected *via* RBC ammonium ions through N–H^+···$^-$OOC (1.89 Å, 163°; 2.05 Å, 149°) hydrogen bonds between the protonated piperazine ring of RBC and the carboxylate anion of VA through a hydrogen-bonded 2D network (Fig. 2b). Water molecules act as bridges to connect these 2D layers *via* O–H···O hydrogen bonds (2.09 Å, 170°; 1.98 Å, 170°) with RBC and VA in a 3D hydrogen-bonded network.

3.1.3. Ribociclib–resorcinol cocrystal (RBC–RES, 1 : 1). RBC–RES crystallized in the space group $P2_1/c$ and its asymmetric unit comprises one molecule each of RBC and resorcinol. RBC molecules are hydrogen bonded to three RES

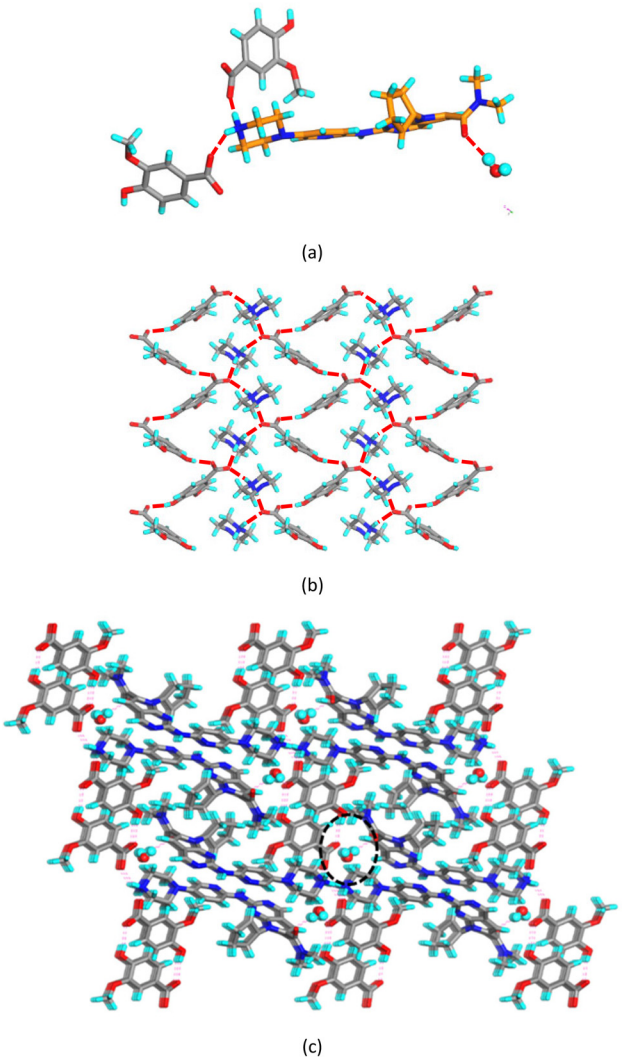

Fig. 2 Crystal structure of RBC–VA–HYD. (a) Hydrogen bonding of RBC, VA ions and water molecules. (b) 2D layered network of hydrogen bonds between protonated RBC and VA anions. Only the piperazinium moiety of RBC is shown for clarity. (c) Hydrogen bonded water molecules in the cavities.

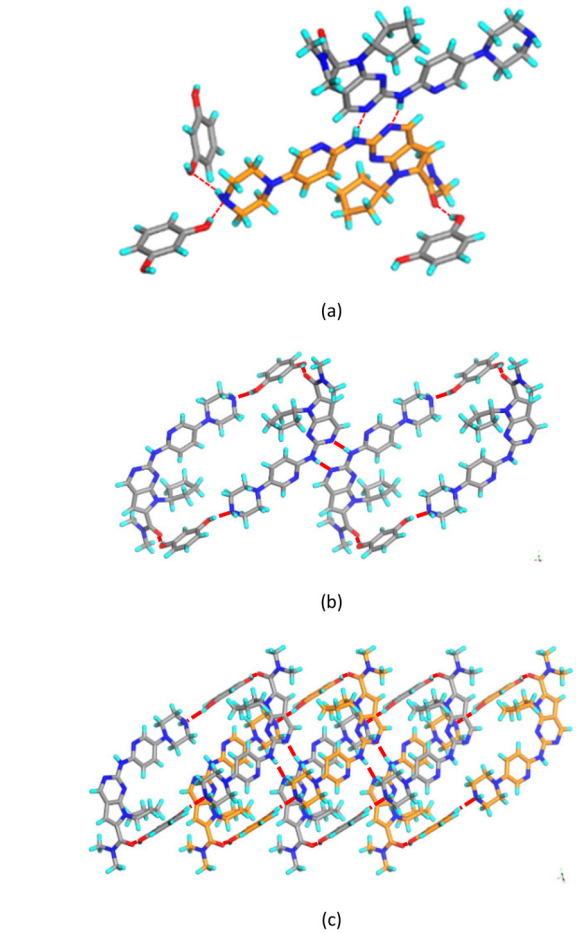

Fig. 3 Crystal structure of RBC–RES. (a) Hydrogen bonding of RBC and RES units; (b) 1D chain formed *via* hydrogen bonding between RES and the self-assembled dimeric unit of RBC; (c) interpenetration of the 1D chains and π–π stacking between pyridine moieties.

molecules and one RBC molecule whereas each RES molecule is hydrogen bonded to three RBC molecules (Fig. 3a). Two molecules of RBC and RES form a hydrogen-bonded cyclic sub-structure *via* O–H···O (1.87 Å, 159°) and O–H···N hydrogen bonds (1.97 Å, 165°). These cyclic units are further connected *via* a N–H···N dimer homosynthon (2.34 Å, 168°) between two RBC molecules with an $R_2^2(8)$ ring synthon, leading to the formation of a 1D chain (Fig. 3b). Such chains propagate through N–H···O hydrogen bonds (2.22 Å, 151°) between the piperazine ring of RBC and the hydroxyl group of RES. The pyridyl rings of RBC are involved in π–π stacking at 3.86 Å distance (Fig. 3c).

3.2. Thermal analysis (DSC and TGA)

Thermal behavior such as melting, desolvation and decomposition of the crystalline adducts was characterized by differential scanning calorimetry (DSC) and thermogravimetric analysis (TGA). The melting points of RBC, RBC hydrate, coformers, the cocrystal and the salt are given in Table 2. The melting endotherm of RBC–HYD (200–201 °C) is very close to that of pure RBC (201–203 °C) (Fig. 4). For RBC–HYD, a broad endotherm in the region of 60–120 °C is due to dehydration for the loss of one water molecule, which was confirmed by TGA (Fig. 5). Finally melting occurred at ~200 °C. In order to confirm if the RBC phase after dehydration is the same as pure RBC (anhydrous), RBC–HYD was heated well beyond the water loss temperature range (~150 °C), cooled to 40 °C, and then reheated to observed that the melting endotherm is at the same temperature as that of pure RBC (201–203 °C). The crystalline nature of this heat–cool phase of RBC–HYD is the same as that of reference RBC by PXRD analysis (see Fig. S5 and S6, ESI†). The RBC–RES cocrystal exhibited a slightly broadened melting endotherm at 237–240 °C, which is higher than the melting points of both the API and the coformer (109–111 °C). Before melting, there was no other endothermic peak in DSC, and no weight loss was observed up to 150 °C in TGA, indicating its non-solvated/non-hydrated nature. The RBC–VA–HYD salt hydrate also showed a higher melting point (217–220 °C) compared to the API and the coformer (210–213 °C). A broad endothermic peak in the range of 40–90 °C, and in TGA, the weight loss in this temperature range confirm the hydrated form. The higher melting temperature of the multicomponent adducts than that of pure RBC and the coformer is due to the stronger and numerous hydrogen bonding networks in the products.

Table 2 Melting points of RBC, RBC–HYD, its salt and cocrystal and coformers

S. No.	Salt	m.p. range (°C)	Coformer	m.p. range (°C)
1	RBC	201–203	—	—
2	RBC–HYD	196–198	—	—
3	RBC–VA–HYD	217–220	VA	210–213
4	RBC–RES	237–240	RES	109–111

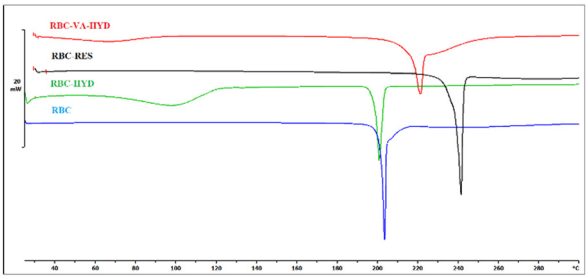

Fig. 4 DSC thermogram of RBC, RBC–HYD and multicomponent solid forms. RBC–VA and RBC–RES show the melting endotherms higher than the melting points of pure RBC and RBC–HYD.

3.3. Solubility and dissolution

Solubility and dissolution are two related properties, based on the thermodynamic and kinetic solubility measurements.[32] Solubility is a thermodynamic property which has an immense impact on the bioavailability of an active pharmaceutical ingredient (API), and this has become one of the major preformulation challenges. From solubility data, it is possible to extract information about the solution phase behavior, which assists in the design of the kinetic study or IDR experiments. For solubility measurement, an excess amount of the drug is dissolved and then phase stability is established at the post equilibrium solubility point of 24 h. The solubility value for RBC is 0.21 mg mL^{-1} (Fig. 6a) and this is similar to the reported value of 0.24 mg mL^{-1}. The PXRD pattern of the residue obtained after the equilibrium solubility experiment confirms that the crystalline form of the drug is stable (Fig. S7, ESI†). The solubility behavior of RBC–HYD remains more or less similar at 0.26 mg mL^{-1} and its phase stability experiment showed conversion to the pure form of RBC (Fig. S8, ESI†). In contrast to the reference drug RBC, the salt and cocrystal exhibited higher solubility. The salt RBC–VA–HYD exhibits a solubility of 0.36 mg mL^{-1} and the cocrystal RBC–RES exhibits even a higher value of 0.44 mg mL^{-1} (Table S4, ESI†). During the equilibrium solubility experiment, the salt is unstable and disproportionated into the initial components (Fig. S9, ESI†), whereas the cocrystal is stable throughout the 24 h equilibrium solubility experiment (Fig. S10, ESI†). The higher solubility of the salt and cocrystal over pure RBC is ascribed to the

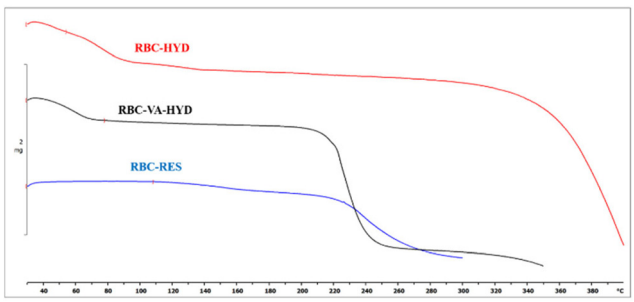

Fig. 5 Thermogravimetric analysis (TGA) of RBC–HYD, the RBC–VA–HYD salt and the RBC–RES cocrystal.

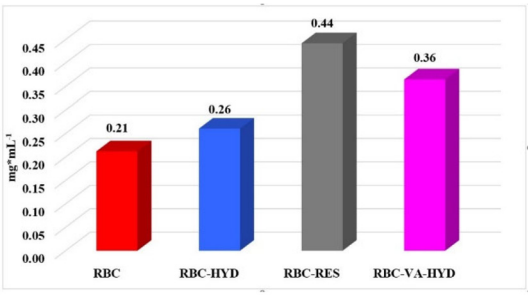

(a)

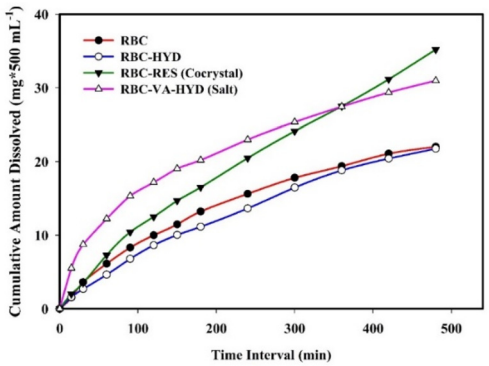

(b)

Fig. 6 (a) Equilibrium solubility comparisons of RBC, RBC-hydrate, the salt-hydrate and the cocrystal in PBS media; (b) cumulative amount dissolved of the API RBC, and its hydrate, salt-hydrate and cocrystal in PBS media.

cocrystallization effect: with VA, the presence of charge-assisted N^+–H···O^- and O–H···O^- hydrogen bonds and with RES, the presence of O–H···N and N–H···O synthons between the drug and coformer, as well as the coformer solubility effect. Consequently, the present cocrystal RBC–RES has high solubility and good solution stability which can be related to the strong hydrogen bonds in the crystal structure, which can provide a lead for the pharmaceutical evaluation and further oral form development.

Studies on the intrinsic dissolution rate (IDR) of the present RBC salt and cocrystal were performed to understand the role of the coformers in modulating the dissolution behavior of the API. The dissolution rate is the rate of mass transfer from the solid surface to the liquid phase under the conditions of a constant surface area, stirring speed, pH and the ionic strength of the dissolution medium. In Fig. 6b, the equimolar ratio of the vanillic acid salt hydrate and resorcinol cocrystal of RBC exhibits faster dissolution rates throughout the time interval of 8 h than the reference drug RBC. Between the VA salt and RES cocrystal,[33] the higher solubility of the coformer RES resulted in higher solubility and a faster dissolution rate (after 6 h) of the RBC–RES cocrystal (Table S5, ESI†).

The water molecules in the salt RBC–VA–HYD structure act as bridges to connect the RBC and VA ions (Fig. 2b), leading to several cavities of the hydrophilic environment internally[34] which can include solvent water and promote faster dissolution (a magnified view is shown in Fig. 2c, to add). However, the salt is not stable and is rapidly disproportionated in PBS media (Fig. S13, ESI†). Therefore, the dissolution rate of the cumulative drug dissolved from the salt hydrate slows down after 6 h compared to the cocrystal (Fig. 6b), because the latter adduct is more stable (Fig. S14, ESI,† the stability of RBC and RBC–HYD at 8 h is shown in Fig. S11 and S12, ESI†). Furthermore, the coformer solubility of RES is much higher than that of VA (82.3 *vs.* 18.6 mg mL^{-1}, Table S4, ESI†). As a result, the increase in solubility/dissolution rate effectively translates into the increased rate and extent of absorption (permeability)[13] for the drug.

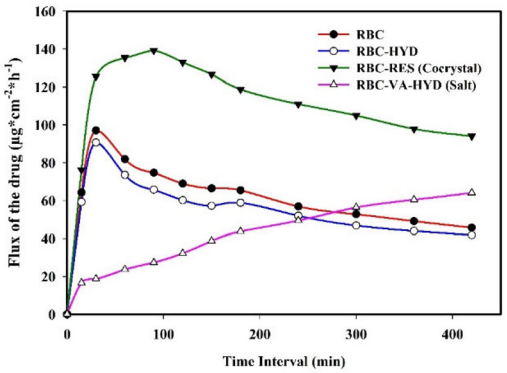

(a)

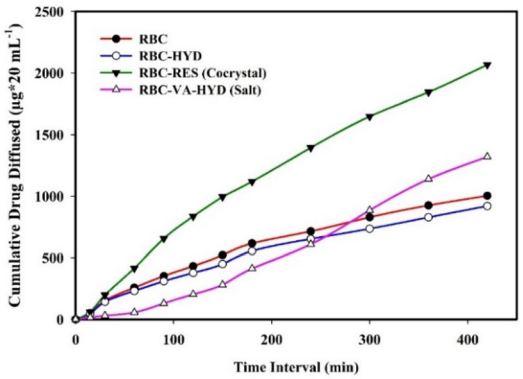

(b)

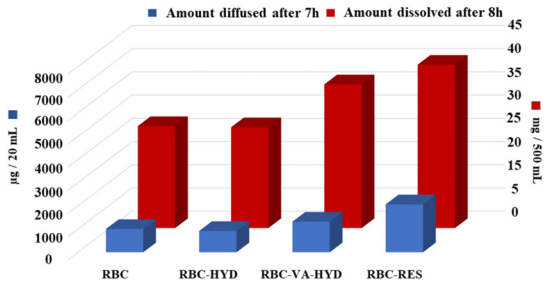

(c)

Fig. 7 (a) Flux *vs.* time plot, (b) cumulative drug diffused *vs.* time plot and (c) comparison of IDR and diffusion for RBC, RBC–HYD, RBC–VA–HYD and RBC–RES (in PBS media).

3.4. Diffusion studies

In addition to high solubility and IDR, the permeability of an API is an important property for high bioavailability.[35] It is important to achieve high solubility and high permeability of the drug in the same crystal form. The Franz diffusion cell plots of the cumulative drug diffused and its flux are shown in Fig. 7a to compare with pure RBC and its hydrate form. The flux passage of the RBC–RES cocrystal exhibited a high rise giving a peak value within 90 min, and then gradually descended to a steady-state corresponding to a constant and unchanged (saturation) membrane crossing of RBC at the basal compartment. In comparison, the salt RBC–VA–HYD showed constant permeation transfer of RBC through the membrane leading to increased concentration throughout the time points. Though there is a constant increase for the salt hydrate of RBC, it has a lower flux rate than the RBC cocrystal. From a cumulative drug absorbed perspective (Fig. 7b), the continuously increasing concentration of RBC can be observed in both the salt and cocrystal of RBC, while the cocrystal presents a remarkably higher cumulative diffused amount (2066 μg cm^{-2}) in 8 h, which is 1.56 times that of the salt (1319 μg cm^{-2}) and 2.06 times higher than that of pure RBC (1002 μg cm^{-2}), demonstrating the enhancement in membrane permeation capacity of RBC in its cocrystal form with RES (Table S6, ESI†). The improvement in permeability of RBC in the cocrystal form can be attributed to the excellent solubility and lipophilic nature of RES which may lead to a higher concentration gradient across the membrane as the driving force. The log*P* value of RES is slightly higher than that of VA (1.37 *vs.* 1.17) but both are lower than that of RBC (2.38). The high solubility and lipophilic nature of the RES coformer resulted in increased dissolution and high membrane permeability of RBC, which show that the solubility–permeability interplay is successfully managed and allows the solubility to be increased without a counter balance of decreased permeability (Fig. 7c).

4. Conclusions

In this study, a salt and a cocrystal of the antineoplastic agent ribociclib were successfully prepared and characterized by single crystal and powder X-ray diffraction, FT-IR spectroscopy and thermal analysis. The drug coformer interactions show that the ionic pair of the RBC–VA–HYD salt is stabilized by charge-assisted N^{+}–H···O^{-} and O–H···O^{-} hydrogen bonds, while the RBC–RES cocrystal is connected *via* neutral N–H···O and O–H···N bonds. The different supramolecular synthons play a decisive role in modifying the solubility and permeability properties of the adducts, which is critical for predicting the resulting solubility and permeability profile of RBC. It is generally believed that solubility and permeability enhancement is a trade-off between hydrophilic (polar functional groups and hydrogen bonding) and hydrophobic factors (lipophilic alkyl and aryl groups). The present results show that the aqueous solubility and membrane permeability are higher for both the salt and cocrystal compared to the reference drug, and that the cocrystal is superior to the salt in terms of the physicochemical properties. The enhanced solubility and permeability of the RES cocrystal are attributed to the higher solubility and lipophilic nature of the coformer and the better stability of the cocrystal, while the lower permeability of RBC–VA–HYD than that of the RBC–RES cocrystal is due to the poor diffusion of its salt form. The present study not only demonstrates that the novel salt and cocrystal of RBC offer structural attributes but also demonstrates that the solubility and the permeability can both be optimized in cocrystals, which provides a better understanding to overcome the poor bioavailability of BCS IV drugs. These observations imply that three properties must be simultaneously optimized in cocrystal–salt screens to enhance drug bioavailability: solubility, permeability and stability.

Author contributions

The manuscript was written through the contributions of all authors. MKCM, AG, and MKB selected the API and optimized coformers to enhance the drug solubility and permeability *via* crystal engineering. KAS and AKN supervised the project and guided the interpretation of data and manuscript writing. All authors have given approval to the final version of the manuscript.

Conflicts of interest

The authors declare no competing financial interest.

Acknowledgements

AKN thanks DST-SERB (JC Bose fellowship, SR/S2/JCB-06/2009 and Pharmaceutical Materials and Continuous Process, CRG/2019/001388) for funding, UGC (through UPE, CAS, NRC and IoE programs) for infrastructure support, DST (through PURSE and FIST programs), and School of Chemistry, University of Hyderabad, for providing instrumentation facilities.

References

1 Novartis Pharmaceuticals, *KISQALI® (Ribociclib) tablets, for oral use: US prescribing Information*, 2017, **https://www.fda.gov**, accessed 31 Mar 2017.
2 C. E. Caldon, R. J. Daly, R. L. Sutherland and E. A. Musgrove, *J. Cell. Biochem.*, 2006, **97**, 261–274.
3 E. Nicolò, D. Trapani, P. P. M. Berton Giachetti, P. Zagami and G. Curigliano, *Cancer Treat. Rev.*, 2021, **100**, 102281.
4 D. Katiyar, S. Ahamad, S. G. Dash, S. Tripathi, A. Arora and T. S. Thakur, *J. Mol. Struct.*, 2021, **1241**, 130637.
5 T. S. Samant, S. Dhuria, Y. Lu, M. Laisney, S. Yang, A. Grandeury, M. Mueller-Zsigmondy, K. Umehara, F. Huth, M. Miller, C. Germa and M. Elmeliegy, *Clin. Pharmacol. Ther.*, 2018, **104**, 374–383.

6 U. Tehler, J. H. Fagerberg, R. Svensson, M. Larhed, P. Artursson and C. A. S. Bergström, *J. Med. Chem.*, 2013, **56**, 2690–2694.
7 G. Bolla, B. Sarma and A. K. Nangia, *Crystal Engineering and Pharmaceutical Crystallization. In Hot Topics in Crystal Engineering*, ed. K. Rissanen, Elsevier, 2021, pp. 157–229.
8 P. Roy and A. Ghosh, *CrystEngComm*, 2020, **22**, 6958–6974.
9 C. A. Hunter and R. Prohens, *CrystEngComm*, 2017, **19**, 23–26.
10 S. K. Rai, S. Allu and A. K. Nangia, *Cryst. Growth Des.*, 2020, **20**, 4512–4522.
11 P. Sanphui, V. K. Devi, D. Clara, N. Malviya, S. Ganguly and G. R. Desiraju, *Mol. Pharmaceutics*, 2015, **12**, 1615–1622.
12 Y. Yan, J.-M. Chen and T.-B. Lu, *CrystEngComm*, 2013, **15**, 6457.
13 V. Ferretti, A. Dalpiaz, V. Bertolasi, L. Ferraro, S. Beggiato, F. Spizzo, E. Spisni and B. Pavan, *Mol. Pharmaceutics*, 2015, **12**, 1501–1511.
14 M. Banik, S. P. Gopi, S. Ganguly and G. R. Desiraju, *Cryst. Growth Des.*, 2016, **16**, 5418–5428.
15 B. Saikia, P. Bora, R. Khatioda and B. Sarma, *Cryst. Growth Des.*, 2015, **15**, 5593–5603.
16 C. R. Groom, I. J. Bruno, M. P. Lightfoot and S. C. Ward, The Cambridge Structural Database, *Acta Crystallogr., Sect. B: Struct. Sci., Cryst. Eng. Mater.*, 2016, **72**, 171–179.
17 *CSD v 2021*, Feb 2021 update, **https://www.ccdc.cam.ac.uk/**, accessed 26 October 2021.
18 *Marvin 5.10.1*, ChemAxon, 2012, **https://www.chemaxon.com**.
19 *Generally Recognized as Safe chemicals by the U.S. FDA*, **https://www.fda.gov/Food/IngredientsPackagingLabeling/FoodAdditivesIngredients/ucm091048.htm**, accessed 03 December 2021.
20 A. J. Cruz-Cabeza, *CrystEngComm*, 2012, **14**, 6362–6365.
21 C. B. Aakeroy, M. E. Fasulo and J. Desper, *Mol. Pharmaceutics*, 2007, **4**, 317–322.
22 S. K. Rai, D. Baidya and A. K. Nangia, *CrystEngComm*, 2021, **23**, 5994–6011.
23 M. S. H. Mithu, S. Economidou, V. Trivedi, S. Bhatt and D. Douroumis, *Cryst. Growth Des.*, 2021, **21**, 1358–1374.
24 P. Sanphui, N. R. Goud, U. B. R. Khandavilli and A. Nangia, *Cryst. Growth Des.*, 2011, **11**, 4135–4145.
25 L. Bofill, D. de Sande, R. Barbas and R. Prohens, *Cryst. Growth Des.*, 2021, **21**, 1418–1423.
26 H. Fael, R. Barbas, R. Prohens, C. Ràfols and E. Fuguet, *Pharmaceutics*, 2022, **14**, 49.
27 G. M. Sheldrick, Crystal Structure Refinement with SHELXL, *Acta Crystallogr., Sect. C: Struct. Chem.*, 2015, **71**, 3–8.
28 *Bruker SMART, Version 5.625, SHELXTL, Version 6.12*, Bruker AXS Inc., Madison, Wisconsin, USA, 2000.
29 A. L. Spek, *Acta Crystallogr., Sect. D: Biol. Crystallogr.*, 2009, **65**, 148–155.
30 T. Higuchi and K. A. Connors, *Adv. Anal. Chem. Instrum.*, 1965, **4**, 117–212.
31 M. C. Etter, J. C. MacDonald and J. Bernstein, *Acta Crystallogr., Sect. B: Struct. Sci.*, 1990, **46**, 256–262.
32 N. Blagden, M. de Matas, P. T. Gavan and P. York, *Adv. Drug Delivery Rev.*, 2007, **59**, 617–630.
33 L. Liu, D. Zou, Y. Zhang, Q. Zhang, Y. Feng, Y. Guo, Y. Liu, X. Zhang, G. Cheng, C. Wang, Y. Zhang, L. Zhang, L. Wu, L. Chang, X. Su, Y. Duan, Y. Zhang and M. Liu, *Eur. J. Pharm. Biopharm.*, 2020, **154**, 62–73.
34 Y.-X. Zhang, L.-Y. Wang, J.-K. Dai, F. Liu, Y.-T. Li, Z.-Y. Wu and C.-W. Yan, *J. Mol. Struct.*, 2019, **1184**, 225–232.
35 Y. Song, L.-Y. Wang, F. Liu, Y.-T. Li, Z.-Y. Wu and C.-W. Yan, *CrystEngComm*, 2019, **21**, 3064–3073.